ARMA 19–371

Effects of fluid diffusivity on hydraulic fracturing processes using visual analysis

Baptista Pereira, C.
New Jersey Institute of Technology, Newark, New Jersey, United States of America
Gonçalves da Silva, B.
New Jersey Institute of Technology, Newark, New Jersey, United States of America

This paper was prepared for presentation at the 53rd US Rock Mechanics/Geomechanics Symposium held in New York, NY, USA, 23–26 June 2019. This paper was selected for presentation at the symposium by an ARMA Technical Program Committee based on a technical and critical review of the paper by a minimum of two technical reviewers. The material, as presented, does not necessarily reflect any position of ARMA, its officers, or members. Electronic reproduction, distribution, or storage of any part of this paper for commercial purposes without the written consent of ARMA is prohibited. Permission to reproduce in print is restricted to an abstract of not more than 200 words; illustrations may not be copied. The abstract must contain conspicuous acknowledgement of where and by whom the paper was presented.

ABSTRACT: Hydraulic fracturing arises as a method to enhance oil and gas production, and also as a way to recover geothermal energy. It is, therefore, essential to understand how injecting a fluid inside a rock reservoir will affect its surroundings. Hydraulic fracturing processes can be strongly affected by the interaction between two mechanisms: the elastic effects caused by the hydraulic pressure applied inside fractures and the poro-mechanical effects caused by the fluid infiltration inside the porous media (i.e. fluid diffusivity); this, in turn, is affected by the injection rate used. The interaction between poro-elastic mechanisms, particularly the effect of the fluid diffusivity, in the hydraulic fracturing processes is not well-understood and is investigated in this paper. This study aims to experimentally and theoretically comprehend the effects of the injection rate on crack propagation and on pore pressures, when flaws pre-fabricated in prismatic gypsum specimens are hydraulically pressurized. In order to accomplish this, laboratory experiments were performed using two injection rates (2 and 20 ml/min), applied by an apparatus consisting of a pressure enclosure with an impermeable membrane in both faces of the specimen, which allowed one to observe the growth of a fluid front from the pre-fabricated flaws to the unsaturated porous media (i.e. rock), before fracturing took place. It was observed that the fracturing pressures and patterns are injection-rate-dependent. This was interpreted to be caused by the different pore pressures that developed in the rock matrix, which resulted from the significantly distinct fluid fronts observed for the two injection rates tested.

1. INTRODUCTION

Hydraulic fracturing arises as a process to enhance oil and gas production or to recover geothermal energy, by injecting pressurized fluid into a wellbore until the target rock fractures, which causes an increase in its permeability. Hydraulic fracturing experienced major technical developments in 1957 (Strain, 1962), but has been more widely used over the world in the last decade and, consequently, its environmental impacts and efficiency.

Among other aspects, it is fundamental to understand the effects of injected fluids on the mechanical and fracturing properties of rocks, as Hubbert and Willis (1957) studied in the context of hydraulic fracturing. Haimson and Fairhurst (1969) studied the relationships between the stresses developed when injecting a fluid inside a porous material and the critical fracturing pressure. However, the injection rate effect was, typically, not investigated in detail.

When a fluid is injected inside existing fractures, or flaws, the pore pressure increases locally, influencing both strength and deformation of the rock (Talwani and Acree, 1984), as well as the magnitudes and orientations of the in-situ stresses (Zhai and Sharma 2007), which may affect the initiation and propagation of fractures. Bruno and Nakagawa (1991) experimentally tested how pore pressure affected tensile fracture initiation and propagation, as well as the orientation of cracks in cylindrical limestone and sandstone samples. They concluded that the crack orientation is influenced by local pressures around the tip and also by the direction of the pore pressure gradients, since fractures developed towards the higher pore pressure regions. Despite extensive experimental and numerical work on this topic, the scientific community has not fully understood the influence of the injection, or pressurization, rate on the damage of rocks (Zhuang et al. 2018).

The current study offers an experimental investigation of the effect of fluid diffusivity on the hydraulic fracturing mechanisms of gypsum using two different injection rates. This paper is organized as follows: Section 2 describes the methodology used during the experiments, including the specimen preparation, the enclosure and test setup used, as well as the procedures followed in the data analysis and numerical modelling. Section 3 describes the results obtained, not only in terms of fracturing pressures but also in terms of the fluid front and fracturing patterns observed. Section 5 provides a summary and conclusions of the study.

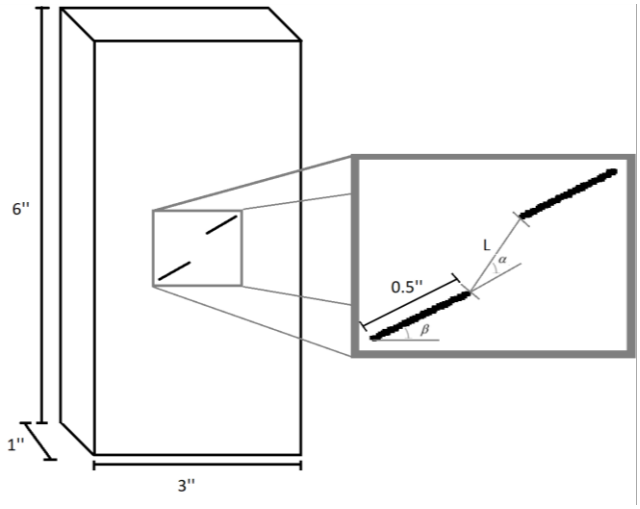

Figure 1: Dimensions of specimen and its pre-fabricated flaws

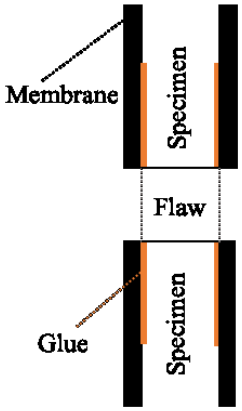

Figure 2: Cross-section of the specimen showing the membrane used to seal the faces of the specimen

2. METHODOLOGY

2.1. Specimen Preparation

The mold to cast the specimens was designed to produce double pre-fabricated flaws with the geometry illustrated in Figure 1. According to Wong (2008), molded gypsum has been successfully used in laboratory experiments as a rock model for the past 50 years given its ease of preparation and, according to Haimson and Fairhurst (1969), because it is a material whose properties are similar to natural rocks. The specimens were cast in accordance to Wong's (2008) work, where the mass ratios of Hydrocal B-11 powder, celite powder and water were 700:8:280. The specimens are removed from the mold one hour after they are cast and then kept in an oven at a temperature of 40 °C in order to evaporate the remaining water. The properties of the gypsum used in these tests are detailed in Table 1, based on the tests conducted by Wong (2008).

Table 1: Properties of the gypsum used in the experiments (Wong, 2008)

Properties	
Poisson ratio, ν $(-)$	0.15
Young's modulus, E (MPa)	5960
Dry density, ρ (g/cm^3)	1.54

2.2. Test setup

In order to initiate and propagate hydraulic fractures from the pre-fabricated flaws, the pressure enclosure described in Gunarathna and Gonçalves da Silva (2019), shown in Figure 3 was used. The specimen was placed inside of a three-plate chamber, with two O-rings to prevent the leakage of the pressurizing fluid, in this case, hydraulic oil. This fluid was injected at two constant rates (2 and 20 ml/min) inside the flaws of the specimen by using a syringe pump.

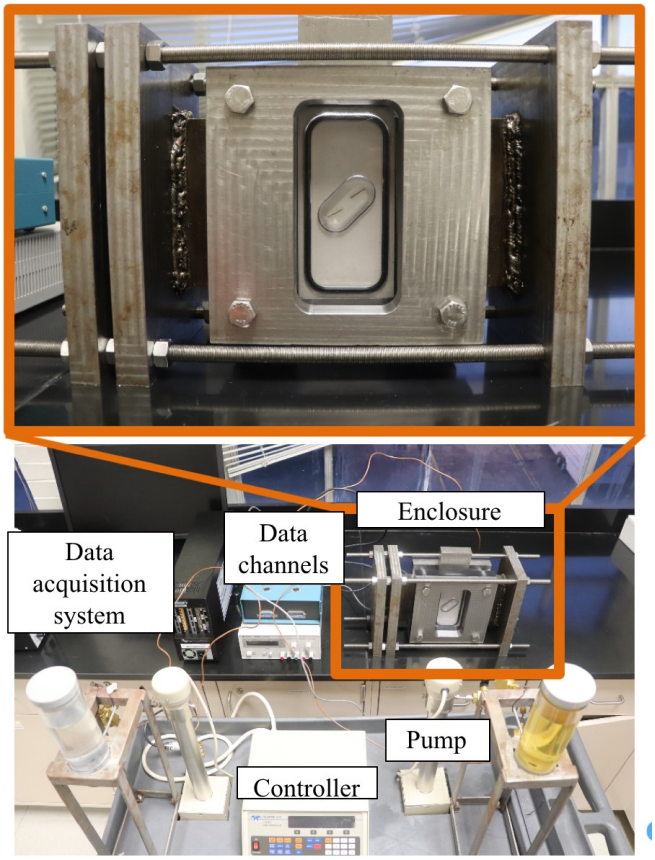

Figure 3: Enclosure and setup used in the experiments

Figure 3 shows the setup used to conduct the experiments: the syringe pump is connected to the back plate of the enclosure to apply the fluid pressure to the flaws. The fluid pressure is measured by a pressure transducer and is

logged by the data acquisition that records these data in real-time.

A transparent plastic membrane is used in the front and back of the faces of the specimen. This membrane allows one to apply the fluid pressure in the internal surfaces of the flaws but not in the faces of the specimen, as shown in Figure 2. By doing this, one can clearly see the growth of the fluid front that propagates due to the diffusivity of the oil.

2.3. Analysis of the experiments

Oil is injected in two pre-fabricated flaws (see Figure 1) and cracks develop due to the 1) increase of pressure inside these flaws and 2) increase in pore pressure in the rock matrix.

The fluid pressures applied in the flaws and the visual observations allow one to determine the pore pressure variation inside the gypsum specimens. In order to estimate these pore pressures and to understand the crack propagation and coalescence, visual analyses are used, based on images captured during the experiments using a high-resolution camera. These images are used to observe the fluid front growth, which allows one to estimate the pore pressure within this front: the pore pressure is assumed zero at the fluid front, $P_{fluid\ front}$, and maximum at the flaw, P_f, which is the pressure being applied by the syringe pump. Between P_f and $P_{fluid\ front}$, the pore pressure is assumed to vary linearly (Figure 4 a). This assumption is made since it is not possible to calculate the real distribution of pore pressure within the fluid front using the current test setup. Points A, B and C are infinitesimal points located, respectively, in the mid-point between inner flaw tips, and at a small distance from the left inner tip. These points will be used to evaluate pore pressures and relate them to the observed fracture initiation and propagation. They were selected based on the fracturing path observed in the tests (discussed in Subsection 3.3).

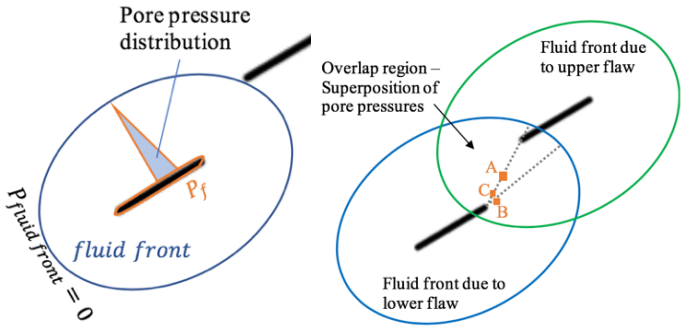

a) b)

Figure 4 a) Assumed variation of pore pressures within the fluid front fluid front and pore pressures for a specific time, t, and b) Influence of fluid fronts and points considered to pore pressure analysis

3. EXPERIMENTAL RESULTS

The study involves the use of four gypsum specimens, two for each injection rate used, whose notation is shown in Table 2.

Table 2 Identification of the gypsum specimens tested

Rate (ml/min)	Specimen 1	Specimen 2
20	GY 20 - 1	GY 20 - 2
2	GY 2 - 1	GY 2 - 2

3.1. Fracturing pressures

The flaw pressure (P_f) variation versus time and volume of oil injected is shown in Figures 5 and 6, respectively.

By analyzing Figure 5, three main stages can be identified:

- The first stage, in which the pressures are close to zero. This corresponds to the filling in of the enclosure;
- The second stage in which the pressures progressively increase and the fluid starts to seep into the rock matrix;
- The third stage when the maximum pressure is reached, fracturing occurs and pressure is almost instantaneously released.

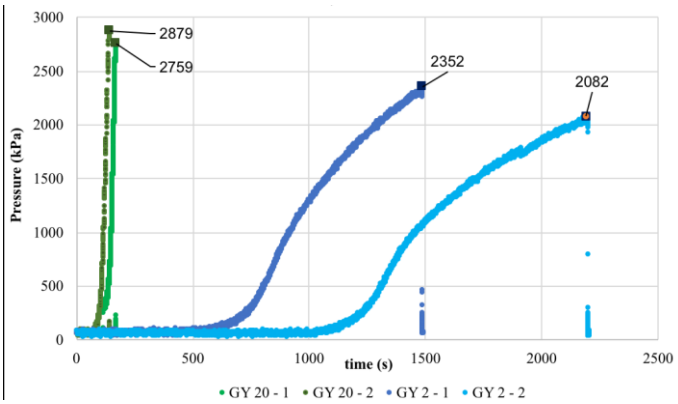

Figure 5: Oil pressure versus time for the four specimens tested using two different injection rates

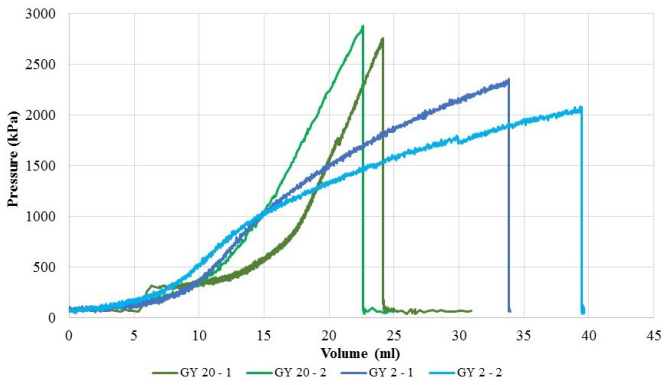

Figure 6: Oil pressure versus volume injected for the four specimens tested using two different injection rates

For a high injection rate, it can be observed that the cracking of the specimens occurs earlier, as intuitively expected. The average fracturing pressures are 2818 kPa and 2217 kPa, for an injection rate of 20 and 2 ml/min, respectively. The low injection rate leads to a lower fracturing pressure due to a more extensive area with increased pore pressures in the bridge between inner flaw tips, as will be further discussed in subsection 3.2.

Figure 6 shows the flaw pressure versus the volume of the injected fluid. Two distinct behaviors can be identified:

- For the low injection rate, the behavior is clearly represented by a smooth negative convexity. This non-linear behavior may be caused by the softening of the gypsum with time, as the oil seeps through the specimen;
- For a high injection rate, the behavior has an abrupt growth, observed by the positive convexity of the curve. As opposed to the lower injection rate, the shape of these curves show that there is an initial adjustment stage in which the stiffness of the gypsum appears to increase followed by an almost perfect linear behavior until failure. Since the high-injection-rate tests are relatively quick (approximately one minute), it appears that the softening behavior observed in the low injection rate tests did not have time to occur here. Finally, it is clear that the volume injected in the high-injection-rate tests is significantly larger (almost twice) than in the low-injection-rate tests.

3.2. Fluid front

Figures 7 and 8 show the development of the fluid front for the two tests conducted with injection rate of 20 ml/min, and Figures 9 and 10 show the development of the fluid front for the two tests conducted with an injection of 2 ml/min. Both injection rates present a uniform fluid front growth with time, which is visible by the darker elliptical shape front of oil - represented in blue and green for the bottom and top flaws, respectively. Please disregard the slightly dark area that is not surrounded by the two elliptical lines, as it corresponds to the glue surface used to attach the membrane to the specimen.

3.3. Comparison between the injection rates of 20 and 2 ml/min

For a high injection rate, the area of the fluid front is relatively small when compared with the lower injection rate, because the fluid does not have enough time to penetrate the pores and diffuse into the specimen. Conversely, for a low injection rate, since the fluid penetrates the specimen at a slower rate, more volume is injected, which results in a much larger fluid front area.

Figures 7 and 8 show the fluid fronts that were used to determine the pore pressures at different times, or flaw pressures shown in Table 3, for the injection rate of 20 ml/min.

Table 3: Fluid pressures inside the flaw, P_f, at different times, for an injection rate of 20 ml/min

	Injection pressure (kPa)	
Times	b)	c)
Figure 7	1292	2759
Figure 8	1168	2879

Figures 9 and 10 show the fluid fronts that were used to determine the pore pressure at different times, or flaw pressures shown in Table 4, for the injection rate of 2 ml/min.

Table 4: Fluid pressures inside the flaw at different times, for an injection rate of 2 ml/min

	Injection pressure (kPa)	
Times	b)	c)
Figure 9	236	2352
Figure 10	230	2082

By comparing Figures 7 and 8 with Figures 9 and 10, one can observe that:

1. The fluid front is much larger for the low injection rate, indicating that a larger volume had to be injected to fracture the rock. This corresponds to what was shown in Figure 6.

2. There is a large overlap of the fluid fronts from both flaws for the injection rate of 2 ml/min, while almost no overlap for the injection rate of 20 ml/min.

As will be discussed, these general observations may explain the differences in fracturing patterns observed.

Using the assumptions explained in Figures 4 a) and b), the average (i.e. of the two tests for each injection rate) pore pressures at points A, B and C are shown in Tables 5 and 6, for the fracturing and intermediate pressures, respectively, as defined in Tables 3 and 4. The pore pressure at point A increases nearly 4.6 times from the

high to the low injection rates, right before cracking takes place. This can be visually observed when one compares Figures 7 and 8, for the high injection rate, with Figures 9 and 10, for the low injection rate. This comparison shows that the dark elliptical areas are more than three times larger for the low injection rate cases. On the other hand, the pore pressures at the inner tips (points B and C) do not show such a significant difference between injection rates, since while at these locations the pore pressures are higher for the low injection rate, this is only by a ratio of nearly 1.4.

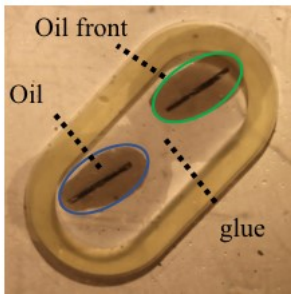

a) Initial time, $P_f = 304\ kPa$

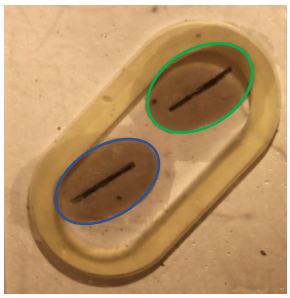

b) Intermediate time, $P_f = 1292\ kPa$

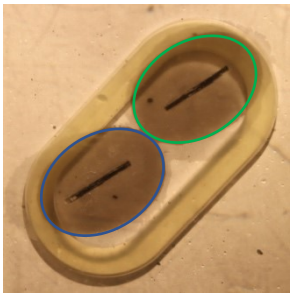

c) Right before cracking occurs, $P_f = 2759\ kPa$

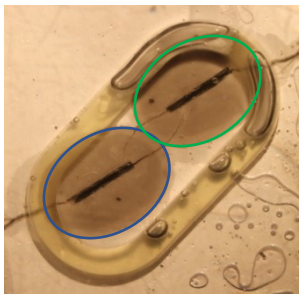

d) Right after cracking occurs, $P_f = 0\ kPa$

Figure 7: Growth of fluid front, when oil is injected at a constant rate of 20 ml/min: GY 20 – 1. The green and blue lines represent the limits of the fluid fronts

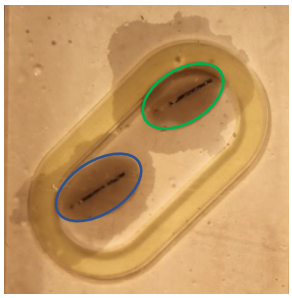

a) Initial time, $P_f = 85\ kPa$

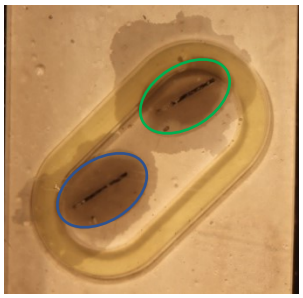

b) Intermediate time, $P_f = 1168kPa$

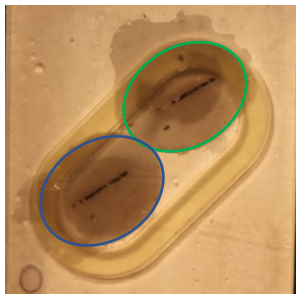

c) Right before cracking occurs, $P_f = 2879\ kPa$

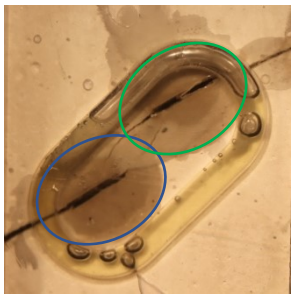

d) Right after cracking occurs, $P_f = 0\ kPa$

Figure 8: Growth of fluid front, when oil is injected at a constant rate of 20 ml/min – GY 20 – 2. The green and blue lines represent the limits of the fluid fronts

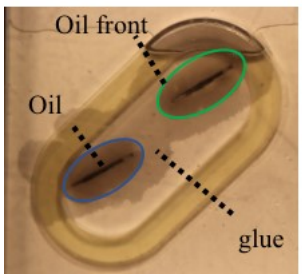

a) Initial time, $P_f = 91\ kPa$

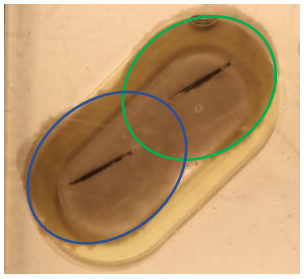

b) Intermediate time, $P_f = 236\ kPa$

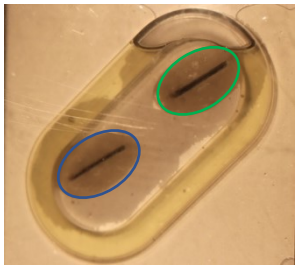

a) Initial time, $P_f = 79\ kPa$

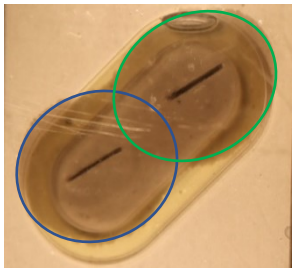

b) intermediate time, $P_f = 230\ kPa$

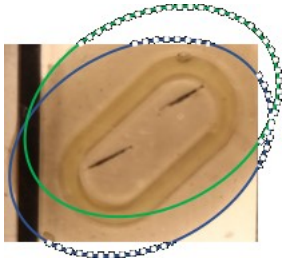

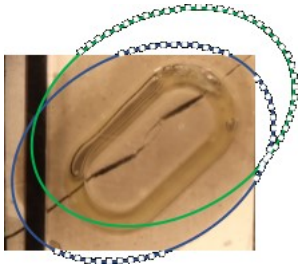

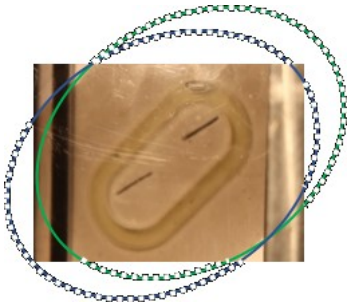

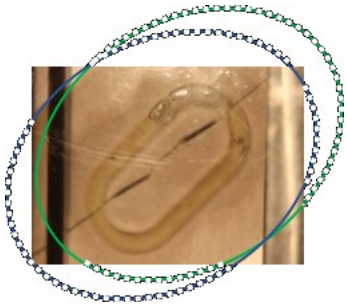

c) Right before cracking occurs, $P_f = 2352\ kPa$

d) Right after cracking occurs, $P_f = 0\ kPa$

Figure 9: Growth of fluid front, when oil is injected at a constant rate of 2 ml/min: GY 2 – 1. The green and blue lines represent the limits of the fluid fronts

c) Right before cracking occurs, $P_f = 2082\ kPa$

d) Right after cracking occurs, $P_f = 0\ kPa$

Figure 10: Growth of fluid front, when oil is injected at a constant rate of 2 ml/min – GY 2 – 2. The green and blue lines represent the limits of the fluid fronts

Comparing now the behavior for the same injection rate, but for the analyzed locations, the pore pressure in the bridge between flaws (point A) is smaller than near the tips (points B and C) when higher injection rates are used because the pore pressures generated in one flaw do not influence the pore pressures generated at the opposite flaw. On the other hand, the pore pressures at point A are similar (slightly larger, in fact) to those at points B and C for the low injection rate, since the pore pressures generated in one flaw strongly affect the pressures at the opposite, leading to higher pore pressures at Point A when pore pressure overlap occurs in the bridge between inner tips.

Table 5: Summary of the pore pressures obtained for each injection rate, at points A, B and C, right before cracking occurred

	Pressure applied (kPa)	pore stresses (kPa)		
		Between flaws, point A	Flaw inner tips, point B	Flaw inner tips, point C
GY 20	2819	822	2718	2723
GY 2	2217	3773	3743	3753

Table 6: Summary of the pore pressures obtained for each injection rate, at points A, B and C, for the intermediate pressure applied

	Pressure applied (kPa)	pore stresses (KPa)		
		Between flaws, point A	Flaw inner tips, point B	Flaw inner tips, point C
GY 20	1230	0	1107	1107
GY 2	233	91	224	225

3.4. Fracturing patterns

The connectivity between the cracks developed from each flaw within the bridge between inner flaw tips is shown from Figures 11 to 14. For the low injection rate, the coalescence occurs directly through a single crack (in one of the tests, with a slight branching into two cracks), while for the high injection rate the coalescence occurs through two cracks which initiate with the same orientation of the flaw.

Using Table 5 in addition to Figures 11 to 14, one can observe that the pore pressures right before cracking are always larger for the low injection rate. This may explain why the cracking, P_f, is lower for the low injection rate; in fact, larger pore pressures will result in a shift of the Mohr circle of stresses in the direction of the tensile strength/envelope of the rock, which indicates that the failure (cracking) of the rock would occur at a lower cracking pressure at the flaw, as experimentally observed.

Furthermore, the different coalescence patters may also be explained by the different pore pressures at points A, B and C. Indeed, for the high injection rate, the pore pressures at point B and C are higher than point A; this indicates that the pore pressure does not have a significant impact in the crack path for the high injection rate and, therefore, the crack is expected to initiate in the same direction as the axis of the flaw based on the linear-elastic stresses around the flaws (see Gonçalves Da Silva and Einstein, 2014), as was experimentally observed is shown in Figure 11 and 12. On the other hand, when the injection rate is low, the pore pressure is higher at points A, B and C, particularly at point A. This indicates that the Mohr circle at point A has a larger shift due to the pore pressure, making it potentially closer to the tensile failure envelope of the rock. Consequently, a cracking path that goes through A appears to be the most compatible with the pore pressures shown in Table 5. This cracking coalescence pattern was, in fact, observed for the low injection rate, as shown in Figures 13 and 14.

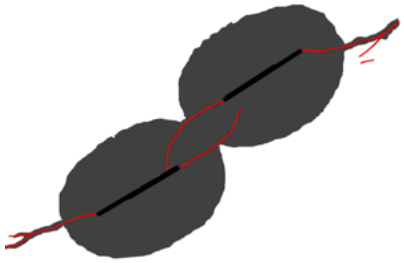

Figure 11: Crack coalescence and fluid front for GY 20 - 1

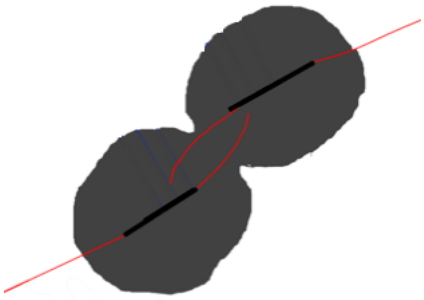

Figure 12: Crack coalescence and fluid front for GY 20 - 2

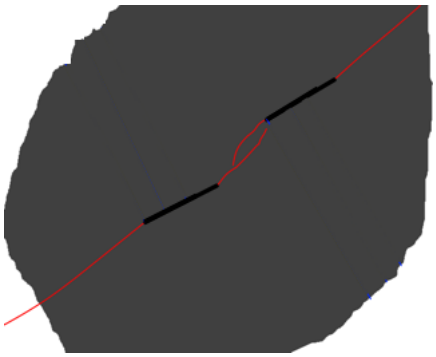

Figure 13: Crack coalescence and fluid front for GY 2 - 1

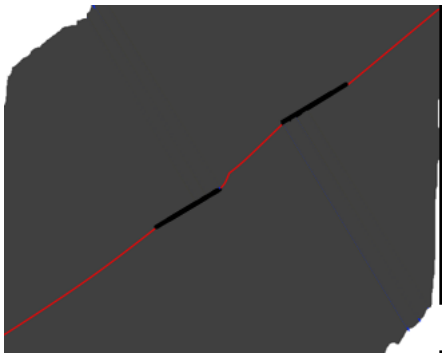

Figure 14: Crack coalescence and fluid front for GY 2 - 2

4. SUMMARY AND CONCLUSIONS

This study investigated the effect of the injection rate on fracturing pressures and patterns, as well as in the pore pressures that develop in the rock matrix through fluid diffusivity.

It was observed that the fracturing pressures were larger for the high injection rate. On the other hand, the fluid front that grew from the flaws, before fracturing took place, was significantly larger for the low injection rate, showing also a major overlap between the fluid fronts originated at each flaw.

The coalescence patterns were also injection-rate dependent. For the low injection rate, coalescence took place through a single crack connecting the flaw tips, while for the high injection rate, the coalescence occurred through two distinct cracks.

The differences in fracturing pressures and patterns were interpreted to be caused by the significant differences between the fluid fronts and, therefore, pore pressures between the high and low injection rates. In fact, the pore pressures that developed in the bridge between inner flaw tips are considerably higher for the low injection rate experiments, which results in a larger shift of the Mohr circle of stresses towards the tensile strength/fracture envelope of the rock.

These theoretical explanations support the experimental observations related to the injection-rate-dependency of the fracturing pressure and patterns.

REFERENCES

Bruno, M.S., and F.M. Nakagawa. 1991. “Pore Pressure Influence on Tensile Fracture Propagation in Sedimentary Rock.” *International Journal of Rock Mechanics and Mining Sciences & Geomechanics Abstracts* 28 (4): 261–73. https://doi.org/https://doi.org/10.1016/0148-9062(91)90593-B.

Gonçalves Da Silva, Bruno, and Herbert H. Einstein. 2014. “Finite Element Study of Fracture Initiation in Flaws Subject to Internal Fluid Pressure and Vertical Stress.” *International Journal of Solids and Structures* 51 (23–24): 4122–36. https://doi.org/10.1016/j.ijsolstr.2014.08.006.

Gunarathna, G., and B. Gonçalves da Silva. 2019. “Experimental Setup Capable of Applying a Triaxial State of Stress While Producing an Imaging Hydraulic Fractures.”

Haimson, Bezalel, and Charles Fairhurst. 1969. “Hydraulic Fracturing in Porous-Permeable Materials.” *Journal of Petroleum Technology* 21 (07): 811–17. https://doi.org/https://doi.org/10.2118/2354-PA.

Hubbert, M. K., and D. G. Willis. 1957. “Mechanics Of

Hydraulic Fracturing." In *Petroleum Branch Fall Meeting in Los Angeles, Oct. 14-17, 1956*, 210:153–68. Society of Petroleum Engineers. https://doi.org/SPE-686-G.

Strain, H. J. 1962. "Well-Bore Notching and Hydraulic Fracturing." *Journal of Canadian Petroleum Technology* 1 (4). https://doi.org/https://doi.org/10.2118/62-04-01.

Wong, L. N. Y. 2008. "Crack Coalescence in Molded Gypsum and Carrara Marble," no. 1999. https://doi.org/10.1007/s00603-008-0002-4.

Zhuang, Li, Kwang Yeom Kim, Sung Gyu Jung, Melvin Diaz, and Ki Bok Min. 2018. "Effect of Water Infiltration, Injection Rate and Anisotropy on Hydraulic Fracturing Behavior of Granite." *Rock Mechanics and Rock Engineering*, no. 1957: 1–15. https://doi.org/10.1007/s00603-018-1431-3.